nature communications

Article

https://doi.org/10.1038/s41467-024-53841-x

# Charge stripe manipulation of superconducting pairing symmetry transition

Received: 25 April 2024

Accepted: 23 October 2024

Published online: 03 November 2024

Check for updates

Chao Chen[1,2,3,8], Peigeng Zhong[2,4,8], Xuelei Sui[2,5], Runyu Ma[1], Ying Liang[1,6], Shijie Hu[1,2] ✉, Tianxing Ma[1,6] ✉, Hai-Qing Lin[1,2,7] & Bing Huang[1,2] ✉

Charge stripes have been widely observed in many different types of unconventional superconductors, holding varying periods ($\mathcal{P}$) and intensities. However, a general understanding on the interplay between charge stripes and superconducting properties is still incomplete. Here, using large-scale unbiased numerical simulations on a general inhomogeneous Hubbard model, we discover that the charge-stripe period $\mathcal{P}$, which is variable in different real material systems, could dictate the pairing symmetries—$d$ wave for $\mathcal{P} \geq 4$, $s$ and $d$ waves for $\mathcal{P} \leq 3$. In the latter, tuning hole doping and charge-stripe amplitude can trigger a $d$-$s$ wave transition and magnetic-correlation shift, where the $d$-wave state converts to a pairing-density wave state, competing with the $s$ wave. These interesting phenomena arise from an unusual stripe-induced selection rule of pairing symmetries around on-stripe region and within inter-stripe region, giving rise to a critical point of $\mathcal{P} = 3$ for the phase transition. In general, our findings offer important insights into the differences in the superconducting pairing mechanisms across many $\mathcal{P}$-dependent superconducting systems, highlighting the decisive role of charge stripe.

Developing the universal understanding of the intertwisting mechanism between different symmetry-breaking orders is one of the most challenging goals in unconventional superconductors. Initially, the emergence of charge orders in a stripe phase was widely discovered in cuprates, e.g., $La_2CuO_4$[1,2], $RBa_2Cu_3O_6$[3], $Bi_2Sr_2CaCu_2O_8$[4], and other family materials, sparking significant interest in their origins[5]. Soon after that, similar charge stripes were later observed in iron-based superconductors, e.g., FeSe[6], and Ni-based superconductors, e.g., infinite-layer nickelates[7–12] and Ruddlesden-Popper-phase nickelates[13]. Very recently, the charge stripes were also found in the kagome-lattice superconductors $CsV_3Sb_5$[14] and $CsCr_3Sb_5$[15]. Clearly, the widespread existence of charge stripes in variable unconventional superconductors highlights their significant role in relation to superconductivity. Interestingly, the period $\mathcal{P}$ and intensity $V_0$ of charge stripe are variable in different materials, which could be tunable by external factors like pressures and defects[16–19], opening potential possibilities to manipulate superconducting pairing symmetry.

Since its inception, the Hubbard model has served as an archetypal model for elucidating strongly correlated phenomena[20,21]. Despite its simplicity, it can uncover rich quantum phases in condensed matter physics[22–28]. For example, the Hubbard model under different conditions can effectively capture $d$-wave pairing symmetry[22,23], stripe order[24–26,29], and antiferromagnetic (AFM) order[28,30] in cuprate-like square lattices, and it can also demonstrate the interplay between these symmetry-breaking orders[31]. Interestingly, previous studies have suggested that the spontaneous formation of

[1]School of Physics and Astronomy, Beijing Normal University, Beijing 100875, China. [2]Beijing Computational Science Research Center, Beijing 100084, China. [3]Department of Basic Courses, Naval University of Engineering, Wuhan 430033, China. [4]School of Physics, Harbin Institute of Technology, Harbin, China. [5]College of Mathematics and Physics, Beijing University of Chemical Technology, Beijing, China. [6]Key Laboratory of Multiscale Spin Physics, Ministry of Education, Beijing, China. [7]School of Physics and Institute for Advance Study in Physics, Zhejiang University, Hangzhou 310058, Zhejiang, China. [8]These authors contributed equally: Chao Chen, Peigeng Zhong. ✉e-mail: shijiehu@csrc.ac.cn; txma@bnu.edu.cn; bing.huang@csrc.ac.cn

charge stripe in a square lattice could be sensitive to variations in model parameters and lattice boundary conditions[32]. Alternatively, the charge stripes can be artificially induced as external fields to explore its relationship with superconductivity. For example, in square-lattice models with $\mathcal{P}=4$ for simulating cuprates, an enhancement of *d*-wave pairing symmetry is observed[33–35] over a broad range of $V_0$, which can be attributed to the intensified AFM correlations between the stripes, accompanied by a $\pi$-phase shift in the system[33]. Until now, however, a comprehensive understanding of the interplay between charge stripe, varying $\mathcal{P}$ and $V_0$ values, and superconducting pairing symmetry remains lacking, which may prevent a deeper insight into the distinct pairing symmetries observed across different systems.

The unbiased determinant quantum Monte Carlo (DQMC) and density-matrix renormalization group (DMRG) methods are widely recognized as two highly accurate and complementary approaches to solving the Hubbard model[22,23,25]. While DQMC can effectively capture the trend of physical quantities at finite temperatures, DMRG is powerful in determining them in the ground state. Here, by combining unbiased DQMC and DMRG simulations on an inhomogeneous square lattice, we discover that the existence of charge stripes with different periods $\mathcal{P}$ [defined in Fig. 1(a)] plays a very unexpected role in determining the pairing-symmetry transition. While the *d*-wave is always dominant for $\mathcal{P}\geq 4$, both *s* (note that this is an extended *s*-wave state afterwards) and *d*-waves can appear when $\mathcal{P}\leq 3$. Taking $\mathcal{P}=3$ as an example, we discover that the interplay between the hole-doping concentration $\delta$ and charge-stripe amplitude $V_0$ can realize a remarkable *d*-*s* wave transition in a large region of the phase diagram, in which the critical $V_0$ ($V_{0,c}$) for the phase transition exhibits a nearly linear dependence of the on-site electron-electron repulsion strength *U*. The DMRG simulations further reveal that the charge-stripe-induced domain wall can generate an interesting selection rule to produce *s* and *d*-waves around the on-stripe region and inside the inter-stripe region, respectively. Therefore, the smaller the $\mathcal{P}$, the stronger the *s*-wave in the system. Accompanying the *d*-*s* wave transition, there is an interesting magnetic-correlation transition, weakening the AFM correlation. These results strongly indicate an inherent interplay between charge stripes, superconducting pairing, and magnetic correlation in the $\mathcal{P}$-dependent systems, in which charge stripes play a vital role in forming the *d*-*s* wave transition.

## Results

### $\mathcal{P}$-dependent *d*-*s* wave transition

In the following, we will mainly discuss the model system with charge stripes at $\mathcal{P}=3$ in a minimal single-$d_{x^2-y^2}$-band Hubbard model, because this simplified model could capture the most intrinsic feature between $\mathcal{P}$ and pairing symmetry and also because a similar dominated role of single-$d_{x^2-y^2}$-band was observed in cuprates and nickelates[36,37]. As shown in Fig. 1(b), we have systematically calculated the pairing-symmetry diagram as a function of $\delta$ and $V_0$. Here, $\delta$ is set to the range of 0.1 ~ 0.3[38,39], and $V_0$ is set to the range of 0 ~ 8 based on the realistic situations. For example, the $V_0$ induced by variable valence Ni charge-state in the stripe of infinite-layer nickelates is estimated to be ~6, which is further tunable under external conditions[17–19]. When $V_0$ is larger than a critical value of $V_{0,c}$ ~3.25, there is a clear pairing-symmetry transition from *d* to *s* waves in a large $\delta$ range of 0.1 ~ 0.23. As will be shown later, this *d*-*s* wave transition is robust against different $U/t$ and $T/t$ values. For comparison, we have also calculated the cases of $\mathcal{P}=2$ and $\mathcal{P}=4$. Interestingly, when $\mathcal{P}=2$, a similar *d*-*s* wave transition can be observed at an even smaller $V_{0,c}$ with a much sharper transition slope (Supplementary Fig. 1). On the other hand, when $\mathcal{P}=4$, only *d*-wave is observed and *d*-*s* wave transition cannot exist in the same $\delta$ range (Supplementary Fig. 2). As summarized in Fig. 1(c), these calculations lead us to an interesting conclusion that $\mathcal{P}=3$ is a critical point for the pairing-symmetry transition, that is, the $\delta/V_0$-dependent *d*-*s* wave transition can only exist when $\mathcal{P}\leq 3$. Importantly, this finding is regardless of whether it is a single-band or multi-band model (Supplementary Fig. 3), being a general feature in $\mathcal{P}$-dependent superconducting systems.

To clearly understand the role of $V_0$ in the *d*-*s* wave transition, we have plotted the $\delta$-dependence of effective pairing interaction $\bar{P}_\alpha$ with the typical parameters of $T=t/5$ and $U/t=4$ under different $V_0$. As shown in Fig. 2(a), without charge stripes ($V_0=0$), $\bar{P}_d$, which is strongest at $\delta=0$, is robust and more stable than that of $\bar{P}_s$ at different $\delta$. Meanwhile, the *s*-wave pairing is suppressed ($\bar{P}_s<0$) at large $\delta$. As shown in Fig. 2(b), when $V_0=3$, $\bar{P}_d$ is rapidly decreased in a much faster way than that of $\bar{P}_s$. This indicates that *s*-wave pairing is more robust against the charge-stripe potential compared to *d*-wave pairing. Importantly, as shown in Fig. 2(c), when $V_0=4$, $\bar{P}_s$ eventually becomes more stable than $\bar{P}_d$ over an extensive $\delta$ range ($0<\delta\leq 0.22$), leading to

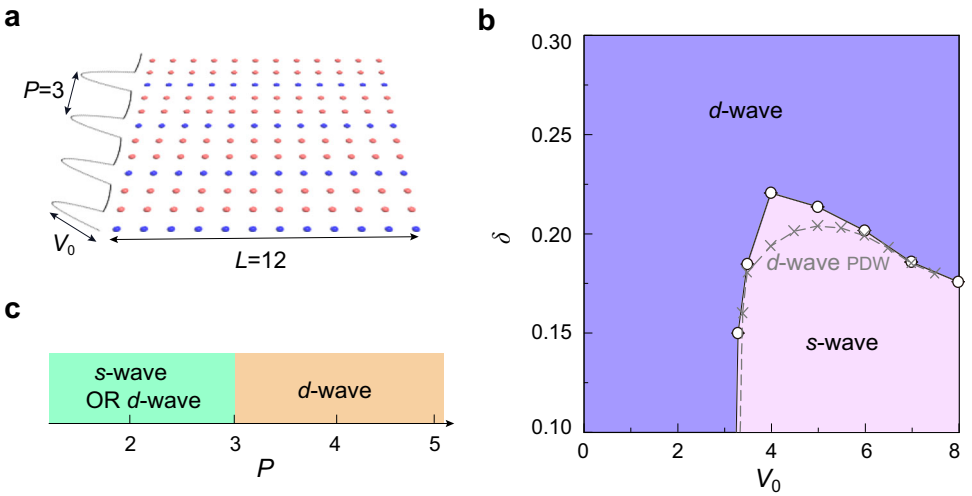


**Fig. 1 | Lattice structure and superconducting phase diagram. a** Geometry of the square lattice with periodic charge stripes. $\mathcal{P}$ denotes charge-stripe period, *L* denotes lattice size, and $V_0$ denotes charge-stripe amplitude. Total number of sites is $N=L\times L$, and $L=12$. Blue (red) circles label the site with (without) the inclusion of $V_0$, representing the on-stripe (inter-stripe) region. **b** Determinant Quantum Monte Carlo (DQMC)-calculated phase diagram of the inhomogeneous Hubbard model with $\mathcal{P}=3$, on-site repulsion strength $U/t=4$, and temperature $T=t/5$, where $t=1$ is the unit of energy. $\delta$ represents hole-doping concentration. Note that the *d*-*s* wave transition is observed even at zero temperature based on density matrix renormalization group (DMRG) simulations. Phase boundary of solid-line is determined by effective pairing strength $\bar{P}_\alpha$ at each ($V_0$, $\delta$). Dashed-line denotes the region where *d*-wave state is transformed into pairing density wave (PDW) state, competing with *s*-wave state. Note that *s*-wave state is always more stable than PDW state. **c** Dominant pairing symmetry depends on $\mathcal{P}$, where $\mathcal{P}=3$ is a critical point.

https://doi.org/10.1038/s41467-024-53841-x

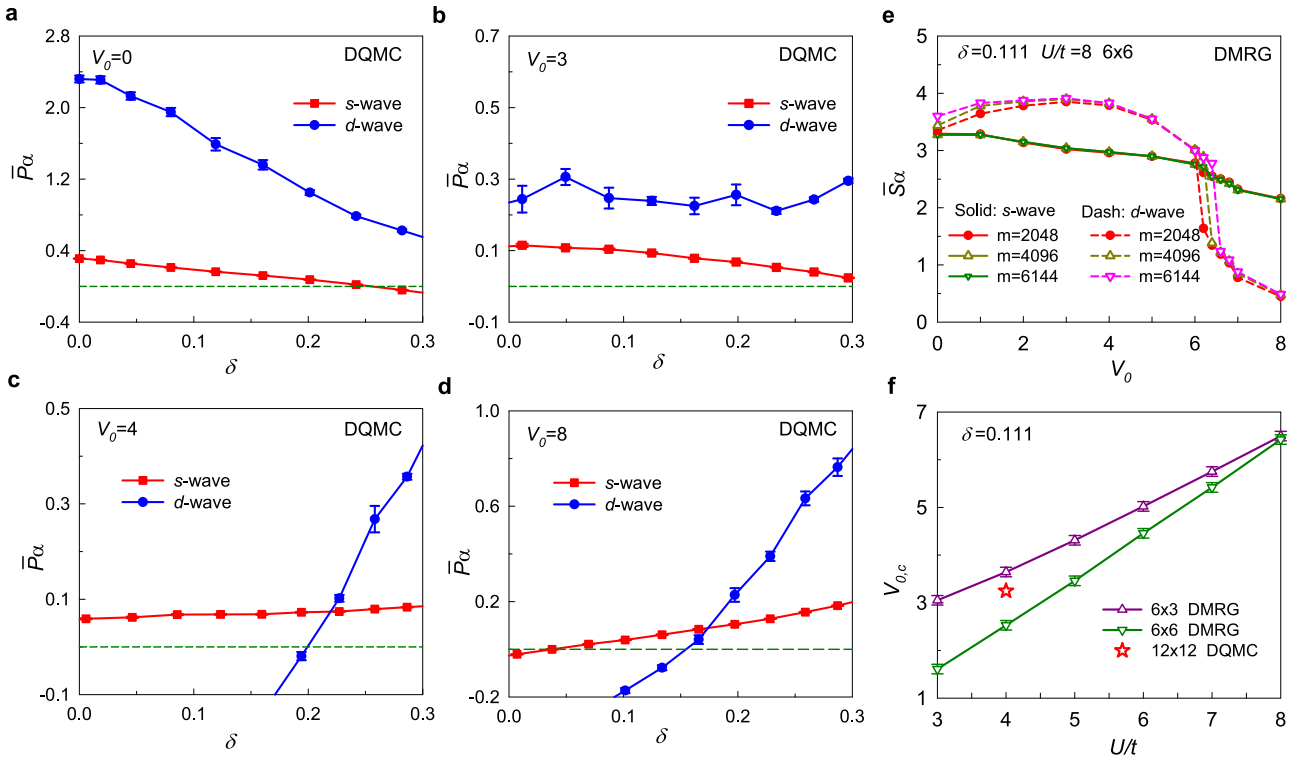


**Fig. 2 | Occurrence of *d*-*s* wave transition.** DQMC-calculated $\bar{P}_\alpha$ as a function of $\delta$ at $T = t/5$ and $U/t = 4$ with $\mathcal{P} = 3$ on a $L = 12$ lattice for (**a**) $V_0$=0, (**b**) $V_0$=3, (**c**) $V_0$=4, and (**d**) $V_0$=8. Here, we divided the data into 10 bins and calculated the error of the data using the jackknife method. The horizontal dashed line represents the zero point on the y-axis. **e** DMRG-calculated effective zero-momentum pair-pair structure factor $\bar{S}_\alpha$ as a function of $V_0$ at $\delta$=0.111 and $U/t = 8$ on the $6 \times 6$ cylinder. While a small discrepancy is observed, it will not affect our conclusion within small error bars. (**f**) DMRG-calculated $V_{0,c}$ for *d*-*s* wave transition with different $U$ on both $6 \times 3$ and $6 \times 6$ cylinders, exhibiting a nearly linear function of $U$. For comparison, DQMC result on a $12 \times 12$ lattice at $U/t = 4$ and $T = t/5$ is also marked here.

a remarkable *d*-*s* wave transition. In particular, *d*-wave pairing is fully suppressed at $0 < \delta \le 0.2$ under $V_0 = 4$, eventually transformed into a *d*-wave PDW state to compete with *s*-wave state, as discussed later. As shown in Fig. 2(d), when $V_0 = 8$, $\bar{P}_s$ maintains more stable than $\bar{P}_d$ in the moderate $\delta$ ($0.05 < \delta \le 0.15$). However, for sufficiently large $\delta$, $\bar{P}_d$ is always more stable than $\bar{P}_s$, regardless of the $V_0$, as also shown in the phase diagram of Fig. 1(b).

The above finite-temperature DQMC conclusion holds at a much lower temperature of $T = t/12$ (Supplementary Fig. 4). To further confirm the ground-state properties at zero temperature, we have systematically calculated effective zero-momentum pair-pair structure factor $\bar{S}_\alpha$ using DMRG method with different cylinders and $U$ (Supplementary Fig. 5). For example, Fig. 2(e) shows $\bar{S}_\alpha$ as a function of $V_0$ at $\delta = 0.111$ and $U/t = 8$ on a $6 \times 6$ cylinder. $\bar{S}_d$ is dominant when $V_0$ is smaller than ~6.2. Interestingly, when $V_0$ is bigger than $\sim 6.2$, $\bar{S}_s$ becomes more robust. Therefore, at ground state, charge inhomogeneity can also support a remarkable *d*-*s* wave transition, demonstrating that the finite-temperature trend obtained from DQMC simulations is reliable at zero temperature. In Fig. 2(f), we have plotted $V_{0,c}$ as a function of $U$ for the observed pairing-symmetry transition with two cylinders. Remarkably, $V_{0,c}$ displays a nearly linear relationship with $U$ for both $6 \times 3$ and $6 \times 6$ cylinders. As $U$ increases, so does $V_{0,c}$, providing a guideline for understanding or manipulating the pairing-symmetry transition. For a typical $U/t = 4$, the DMRG-calculated $V_{0,c}$ in $6 \times 3$ and $6 \times 6$ cylinders exhibit slightly different values indicating the lattice-size dependence. However, these values are overall consistent with DQMC results. Therefore, our results undisputedly demonstrate that this *d*-*s* wave transition exists in a $\mathcal{P} = 3$ system and that the $V_{0,c}$ depends on $U$.

We have further investigated the critical role of different parameters on $\bar{P}_\alpha$. Here, we choose the cases of $\delta = 0.3$ (*d*-wave-dominated region) and $\delta = 0.18$ (*s*-wave-dominated region). Figure 3(a)–(b) show the case of *d*-wave pairing at $\delta = 0.3$. In Fig. 3(a), we calculate the temperature-dependent $\bar{P}_d$ for different $V_0$. As temperature is lowered, $\bar{P}_d$ increases rapidly. Importantly, it is observed that *d*-wave pairing is enhanced with the increase of $V_0$, indicating the important role of charge fluctuation[31,33]. This enhancement may be caused by the appearance of more nearly half-filled inter-stripe regions for larger $V_0$ at $\delta = 0.3$ (Supplementary Fig. 6). On the other hand, Fig. 3(b) shows that the $\bar{P}_d$ is enhanced by larger $U$, suggesting the importance of electron-electron correlation. Importantly, the lattice size effect of $\bar{P}_d$ is weak, i.e., $L = 9$, 12, and 15 exhibit almost identical results.

Figure 3 (c)–(d) show the case of *s*-wave pairing at $\delta = 0.18$. In Fig. 3(c), we present the temperature dependence of $\bar{P}_s$, in which $\bar{P}_d$ is also plotted here for comparison. For $V_0 = 5 \sim 7$, $\bar{P}_s$ is positive and increases slowly with decreasing temperature. The larger $V_0$, the stronger $\bar{P}_s$. However, $\bar{P}_d$ is negative at $V_0 = 5$ ~ 6 and becomes positive at $V_0 = 7$. So, below $V_0 = 7$, $\bar{P}_d$ is less stable than $\bar{P}_s$ at all the considered temperature ranges. It is curious to understand the origin of the suppression of *d*-wave state, which suggests that there may be an unusual phase transition. To confirm our speculation, we have systematically calculated the possible PDW state in $\mathcal{P} = 3$ system. Taking $V_0 = 5$ as an example [Fig. 3(c)], interestingly, the peak of $P_d^{\mathrm{PDW}}(\mathbf{q})$ moves away from zero momentum and the system shows a tendency to form a PDW state. Although $P_d^{\mathrm{PDW}}(\mathbf{q})$ is positive, it is still less stable than $\bar{P}_s$. In addition, we further calculate the competition between $P_d^{\mathrm{PDW}}(\mathbf{q})$ and $\bar{P}_s$ under different $V_0$ and $\delta$ (Supplementary Fig. 7), and find that *s*-wave state is always more stable than PDW state. This may account for the challenge to observe PDW in nickelates, whch is hidden behind the *s*-wave. In the phase diagram of Fig. 1(b), we have also plotted the boundary where PDW states emerge, which is close to the boundary of

https://doi.org/10.1038/s41467-024-53841-x

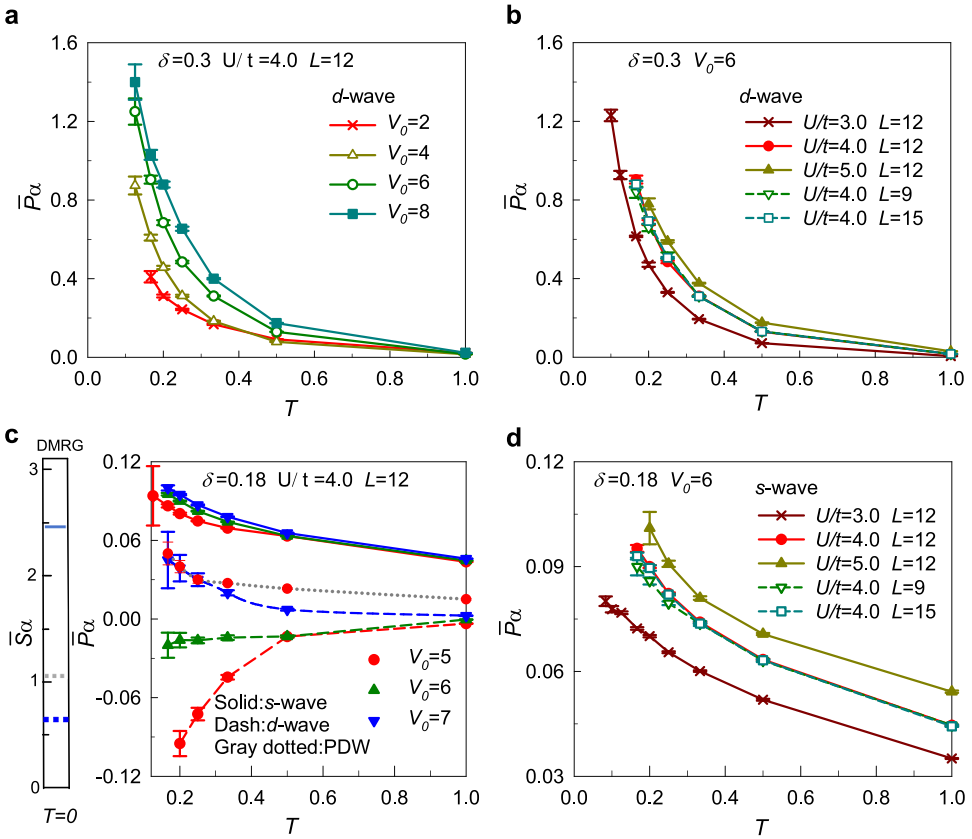


**Fig. 3 | Effective pairing interactions and structure factors.** DQMC-calculated $\bar{P}_\alpha$ as a function of temperature (**a**) for different $V_0$ at $\delta = 0.3$, $U/t = 4$, and $L = 12$, (**b**) for different $U/t$ or $L$ at $\delta = 0.3$ and $V_0 = 6$. **c**–**d** are similar to (**a**–**b**) but for the cases of $\delta = 0.18$. Gray-dotted line in (**c**) represents the $d$-wave PDW at $V_0 = 5$. Left of (c): DMRG-calculated $\bar{S}_\alpha$ of $s$-wave (blue-solid) and $d$-wave (blue-dash), and the peak value of $d$-wave PDW $\bar{S}_d(\mathbf{q})$ (gray-dash) at $\delta = 0.111$, $U/t = 8$, $V_0 = 7$ on a $6 \times 6$ cylinder. The error of the DQMC data are calculated by using the jackknife method.

$s$-wave state. To further confirm our DQMC conclusion, we have plotted DMRG-calculated $\bar{S}_\alpha$ of the $s$- and $d$-waves, and the peak value of PDW $\bar{S}_d(\mathbf{q})$ at $\delta = 0.111$, $U/t = 8$, $V_0 = 7$ on a $6 \times 6$ cylinder, supporting the dominance of $s$-wave at zero temperature (see more cases in Supplementary Fig. 8). Figure 3(d) shows $\bar{P}_s$ as a function of temperature at different $U$ and $L$. Similar to that in Fig. 3(b), it is obvious that $\bar{P}_s$ is also enhanced with increasing $U$ and shows a very weak lattice-size effect. Furthermore, our constrained path quantum Monte Carlo (CPQMC) and DMRG simulations also suggest the possible emergence of long-range $s$-wave superconducting order within the investigated parameter region (Supplementary Fig. 9 and Supplementary Fig. 10).

## Origin of *d*-*s* wave transition

It is interesting to understand the physics insight behind this $d$-$s$ pairing-symmetry transition. In Fig. 4, based on the ground-state DMRG analysis on the condensate wave function, we realize that this phase transition is strongly related to charge-stripe-induced potential fluctuation, where the domain-walls can form around the on-stripe region (blue-circle in Fig. 4). Specifically, the DMRG-calculated dominant Cooper pair mode $\zeta_0(\mathbf{i}\boldsymbol{\delta}_l)$ supports that a clear local pattern of $s$-wave pairing can emerge around on-stripe regions at moderate $V_0$ and $\delta$, regardless of $\mathcal{P}$, where horizontal and vertical bonds have the same signs (Supplementary Fig. 11). On the contrary, inter-stripe region (red-circle in Fig. 4) is always beneficial to asymmetric $d$-wave, as long as $\mathcal{P}$ is sufficiently large, where horizontal and vertical bonds exhibit opposite signs (Supplementary Fig. 11). In brief, without the domain-wall, the system favors asymmetric $d$-wave patterns. In the presence of domain-walls, the influence of domain-walls on pairing symmetry is local, and $s$-wave patterns can only be prominent near on-stripe region at moderate $V_0$ and $\delta$. The smaller $\mathcal{P}$, the more the $s$-wave components can be generated in the system. When $\mathcal{P} \geq 4$, the inter-stripe $d$-wave region plays a dominant role in forming global $d$-wave pairing in the system. However, when $\mathcal{P} \leq 3$, the intensity of $s$-wave pattern near on-stripe region is sufficiently strong to convert the global pairing symmetry from $d$ to $s$. This understanding not only can explain why the $d$-$s$ wave transition is more accessible in a smaller $\mathcal{P}$ system [Supplementary Fig. 1 and Fig. 1(c)], but also suggests that the local $s$-wave pairing may also exist in $\mathcal{P} \geq 4$ ($d$-wave-dominant) systems, as long as the $V_0$ and $\delta$ are in a suitable region.

Besides the pairing-symmetry transition, it is also curious to understand the role of charge stripe on the modulation of spin susceptibility [$\chi_s(\mathbf{q})$]. In Figs. 5(a) and (b), we have calculated the $\chi_s(\mathbf{q})$ for two different $V_0$ at $\delta = 0.3$ in the $\mathbf{q}$-space (see more $V_0$ cases in Supplementary Fig. 12). In the $d$-wave region, the system behaves as the AFM correlation. One can see that the $(\pi, \pi)$ magnetic correlation is enhanced as the $V_0$ increases, i.e., the system exhibits a stronger AFM fluctuation along the direction of stripes ($x$ direction) with larger $V_0$. This AFM-correlation enhancement is possibly caused by more nearly half-filled inter-stripe regions (Supplementary Fig. 6), similar to the behavior of enhanced $d$ pairing symmetry at $\delta = 0.3$. Moreover, subpeaks emerge at $q_y = \pi \pm \pi/\mathcal{P} = 2\pi/3$ and $4\pi/3$, reflecting the incommensurate spin correlations observed in the $d$-wave superconductor[29], and are gradually suppressed as increasing $V_0$ from 4 to 6.

The case is dramatically changed in the $s$-wave region. In Fig. 5(c) and (d), we have calculated $\chi_s(\mathbf{q})$ at $\delta = 0.18$ with two different $V_0$, in which the $s$-wave pairing symmetry is dominated. Surprisingly, along with the $d$-$s$ wave transition, the AFM correlation at $(\pi, \pi)$ is weakened.

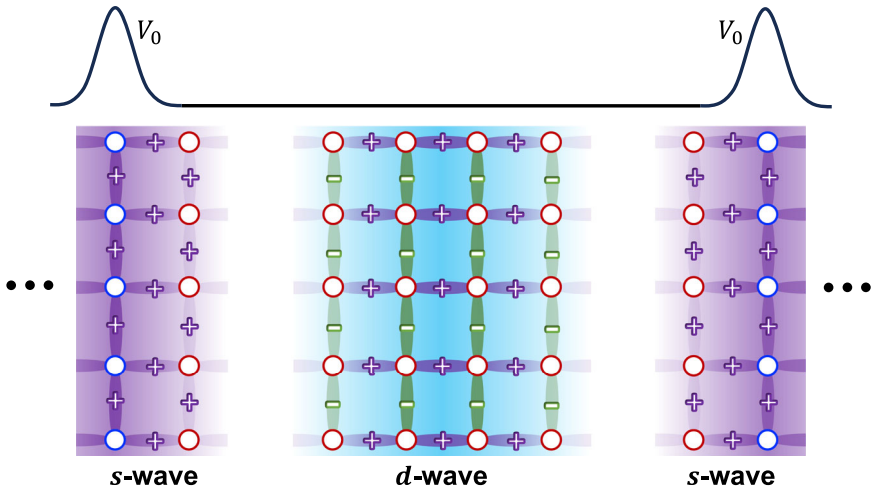


**Fig. 4 | Physical Origin of the *d*-*s* wave transition.** Sketch depicts the *d*-*s* wave transition by analyzing the condensate wave function of the dominant Cooper pair mode $\zeta_0(\mathbf{i}\boldsymbol{\delta}_l)$ based on DMRG simulations. Blue (red) circles label the sites in the on-stripe (inter-stripe) region with (without) $V_0$. Purple (green) bonds indicate positive (negative) values of $\zeta_0(\mathbf{i}\boldsymbol{\delta}_l)$. The solid line at the top illustrates the magnitude of the striped potential energy. Symmetric *s*-wave patterns only occur near on-stripe regions (domain-walls) at moderate $V_0$ and $\delta$, i.e., horizontal and vertical bonds have the same signs. On the contrary, the inter-stripe region always benefits asymmetric *d*-wave, i.e., horizontal and vertical bonds have opposite signs. Due to the competition between the *d*- and *s*-wave pairing symmetries, global *s*-wave pattern can be stabilized with $\mathcal{P} \le 3$.

In detail, $\chi_s(\mathbf{q})$ shows a dumbbell shape, different from the rod shape for the *d*-wave at $\delta = 0.3$. The dumbbell distribution becomes more obvious as $V_0$ increases (see more $V_0$ cases in Supplementary Fig. 13). Besides, the $(\pi, \pi)$ magnetic correlation and dominant pairing correlation exhibit a very similar temperature dependence (Supplementary Fig. 14). Given that magnetism and superconductivity simultaneously exhibit dramatical differences in these two doping cases of $\delta = 0.3$ and 0.18, it indicates that the pairing-symmetry transition and magnetic-correlation transition are strongly interwoven.

## Discussion

Both charge and spin stripes are widely observed in many superconductors. Although the spin stripe itself is interesting in a model study, it is beyond the focus for our current study. Meanwhile, although the major conclusion is described by a minimal Hubbard model, it is robust against the multi-band model (Supplementary Fig. 3) or different stripe styles (Supplementary Fig. 15). Since the charge stripe in a real material system might be tunable under some external conditions, combined with the linear relationship between $V_{0,c}$ and $U$, our study provides an interesting idea of charge-stripe engineering of pairing symmetry. During the *d*-*s* wave phase transition, the competition between PDW and *s*-wave provides an important opportunity to explore the exotic intertwining phenomenon between PDW, *d*-wave, and *s*-wave.

## Methods

The two-dimensional Hubbard Hamiltonian on a square lattice with nearest-neighbor hopping $t$ and Coulomb repulsion $U$ is written as

$$\begin{aligned}\hat{H} = & -t\sum_{\langle \mathbf{i},\mathbf{j}\rangle\sigma}(c^{\dagger}_{\mathbf{i}\sigma}c_{\mathbf{j}\sigma} + c^{\dagger}_{\mathbf{j}\sigma}c_{\mathbf{i}\sigma}) + U\sum_{\mathbf{i}} n_{\mathbf{i}\uparrow}n_{\mathbf{i}\downarrow} \\ & -\mu\sum_{\mathbf{i}}(n_{\mathbf{i}\uparrow} + n_{\mathbf{i}\downarrow}) + V_0\sum_{mod(i_y,\mathcal{P})=0}(n_{\mathbf{i}\uparrow} + n_{\mathbf{i}\downarrow}).\end{aligned} \tag{1}$$

Here, $c_{\mathbf{i}\sigma}$ ($c^{\dagger}_{\mathbf{i}\sigma}$) annihilates (creates) electrons at site $\mathbf{i}$ with spin $\sigma$ ($\sigma = \uparrow, \downarrow$), and $n_{\mathbf{i}\sigma} = c^{\dagger}_{\mathbf{i}\sigma}c_{\mathbf{i}\sigma}$ is the particle number operator for the electron. We set the nearest-neighbor hopping $t = 1$ as the energy unit. $\mu$ is a global chemical potential for all sites, and $V_0$ is an additional potential exerted on a set of on-stripe rows $\mathbf{i} = (i_x, i_y)$ where $i_y = 0$ modulo $\mathcal{P}$, that is, $\mathrm{mod}(i_y, \mathcal{P}) = 0$. The larger $V_0$, the stronger the charge fluctuation. Accordingly, as shown in Fig. 1(a), the charge stripe with tunable oscillation strength can be introduced externally via a raised energy $V_0$. To further confirm our results, we have also selected a cosine-like varying modulation (Supplementary Fig. 15). Interestingly, $V_{0,c}$ for the *d*-*s* wave transition becomes even smaller when we choose the cosine-like varying charge modulation.

We note that the purpose of this model is not to address the origin of the stripe formation, as this is still an open question. Instead, it allows us to estimate the characteristics of spin and pairing correlations in the presence of pre-existing charge orders. This is an appropriate approximate model when the energy scale of the stripe formation is greater than that of superconductivity[31,33,35,38–41].

### DQMC method

Our calculations are mainly performed on the lattice shown in Fig. 1(a) using the DQMC method with periodic boundary conditions. This unbiased numerical method is powerful and reliable to investigate strongly-correlated electrons[42–46]. The basic strategy of the finite-temperature DQMC method is to express the partition function $Z = \mathrm{Tr}\exp(-\beta H)$ as a high-dimensional integral over a set of random auxiliary fields. The integration is then accomplished by Monte Carlo sampling. In our DQMC simulations, 8000 warm-up sweeps are conducted to equilibrate the system, and an additional 10,000 ~ 1,200,000 sweeps are performed for measurements, which are divided into 10 ~ 20 bins. Besides, two local updates are performed between measurements. In the process of eliminating the on-site interaction, the inverse temperature $\beta = 1/T$ is discretized. And the discretization mesh $\Delta\tau = 0.1$ of $\beta$ is chosen small enough so that the resulting Trotter errors are typically smaller than those associated with the statistical sampling.

We have performed a systematical analysis of the infamous sign problem[46] in our DQMC simulations. The average sign decreases quickly as the inverse temperature exceeds 3, and the sign problem gets worse for higher $U$ and larger $L$. In most of our calculations, the average sign keeps as $> 0.55$ (see Supplementary Fig. 16). In order to explore the lower temperature behavior of $\bar{P}_{\alpha}$, the average sign keeps as $> 0.4$ (Supplementary Fig. 17). In short, the conclusions obtained from our DQMC calculations are reliable.

https://doi.org/10.1038/s41467-024-53841-x

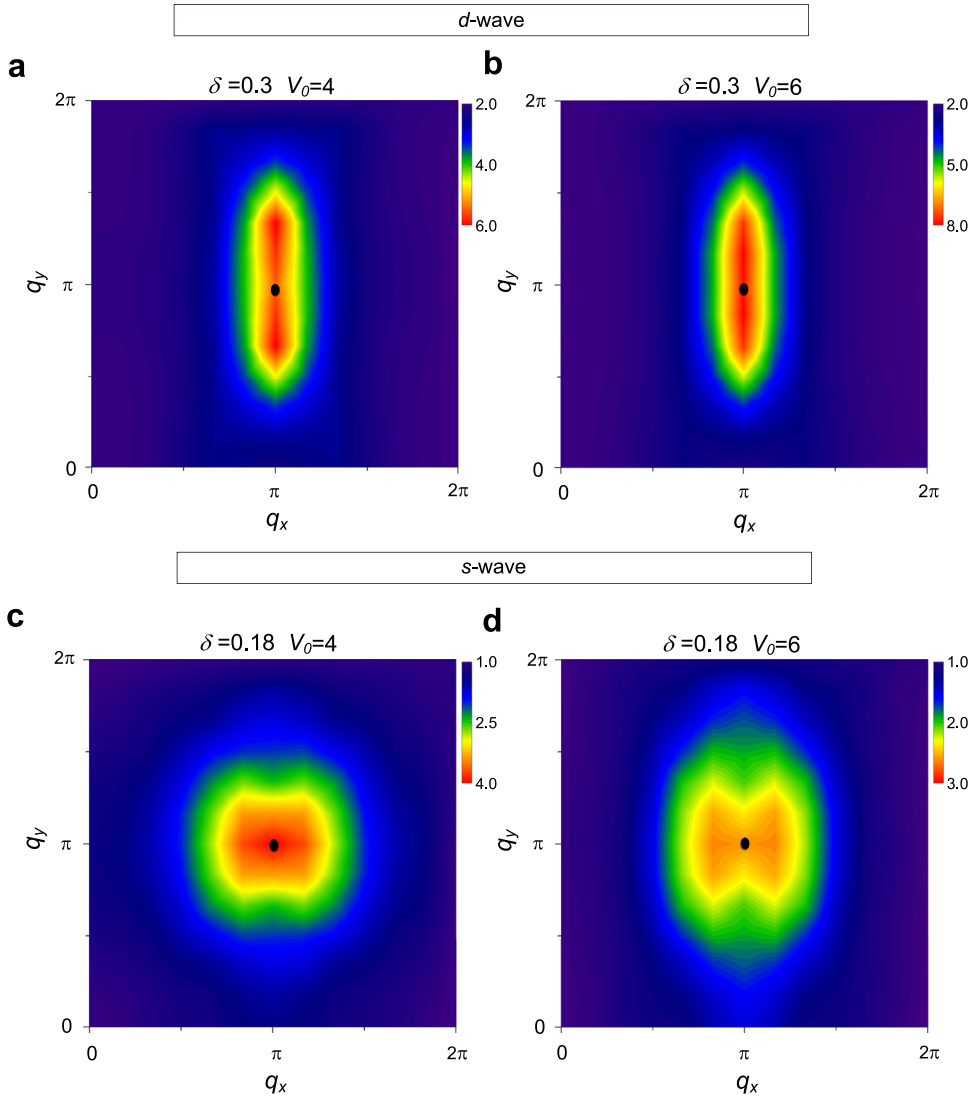


**Fig. 5 | Correlation between spin susceptibility and magnetism.** DQMC-calculated spin susceptibility $\chi_s(\mathbf{q})$ in the first Brillouin zone at $T = t/5$, $U/t = 4$ with (**a**) $\delta = 0.3$ and $V_0 = 4$, (**b**) $\delta = 0.3$ and $V_0 = 6$, (**c**) $\delta = 0.18$ and $V_0 = 4$, and (**d**) $\delta = 0.18$ and $V_0 = 6$. Here, (**a**–**b**) are for the *d*-wave cases, and (**c**–**d**) are for the *s*-wave cases.

To explore the effects of the charge-density modulation on superconductivity, we define the pairing interaction as

$$P_\alpha = \frac{1}{N_s}\sum_{\mathbf{i},\mathbf{j}} \mathcal{D}_\alpha(\mathbf{i},\mathbf{j}), \tag{2}$$

where

$$\mathcal{D}_\alpha(\mathbf{i},\mathbf{j}) = \int_0^\beta d\tau \left\langle \Delta_\alpha^\dagger(\mathbf{i},\tau)\Delta_\alpha(\mathbf{j},0)\right\rangle_T \tag{3}$$

gives the zero-frequency pair-pair correlation function between sites $\mathbf{i}$ and $\mathbf{j}$, $\alpha$ represents the pairing symmetry, the corresponding order parameter $\Delta_\alpha(\mathbf{i},\tau) = e^{H\tau}\Delta_\alpha(\mathbf{i},0)e^{-H\tau}$ and $\Delta_\alpha^\dagger(\mathbf{i},0)$ is written as

$$\Delta_\alpha^\dagger(\mathbf{i},0) = \sum_l f_\alpha^*(\boldsymbol{\delta}_l)\mathcal{C}_{\mathbf{i}\boldsymbol{\delta}_l}^\dagger \tag{4}$$

with $\mathcal{C}_{\mathbf{i}\boldsymbol{\delta}_l} = c_{\mathbf{i}\uparrow}c_{\mathbf{i}+\boldsymbol{\delta}_l\downarrow} - c_{\mathbf{i}\downarrow}c_{\mathbf{i}+\boldsymbol{\delta}_l\uparrow}$ denoting the operator for the Cooper pair on the sites $\mathbf{i}$ and $\mathbf{i}+\boldsymbol{\delta}_l$, and $f_\alpha(\boldsymbol{\delta}_l)$ stands for the form factor of pairing function. The vectors $\boldsymbol{\delta}_l$ ($l$ =1, 2, 3, 4) denote the nearest-neighbor connections, and $\boldsymbol{\delta}_l$ is $\pm\hat{x}$ and $\pm\hat{y}$. Considering the structure of the square lattice, the possible singlet pairing forms are given by either the extended *s*-wave or the *d*-wave, which have the following form factor[33,47],

$$\begin{aligned} s-\text{ wave}&: \mathrm{f_s}(\boldsymbol{\delta}_\mathrm{l}) = +1,\\ d-\text{ wave}&: \mathrm{f_d}(\boldsymbol{\delta}_\mathrm{l}) = \begin{cases} +1 \text{ for } \boldsymbol{\delta}_\mathrm{l} = \pm\hat{\mathrm{x}} \\ -1 \text{ for } \boldsymbol{\delta}_\mathrm{l} = \pm\hat{\mathrm{y}} \end{cases}, \end{aligned} \tag{5}$$

In practice, the effective pairing interaction $\bar{P}_\alpha$ is a more direct probe to identify the dominant superconducting pairing form[48,49]. In order to obtain $\bar{P}_\alpha$, the uncorrelated single-particle contribution $\bar{\mathcal{D}}_\alpha(\mathbf{i},\mathbf{j})$ is also calculated, which is reached by replacing $\langle c_{\mathbf{i}\downarrow}^\dagger c_{\mathbf{j}\downarrow} c_{\mathbf{i}+\boldsymbol{\delta}_l\uparrow}^\dagger c_{\mathbf{j}+\boldsymbol{\delta}_{l'}\uparrow}\rangle$ in Eq. (2) with $\langle c_{\mathbf{i}\downarrow}^\dagger c_{\mathbf{j}\downarrow}\rangle\langle c_{\mathbf{i}+\boldsymbol{\delta}_l\uparrow}^\dagger c_{\mathbf{j}+\boldsymbol{\delta}_{l'}\uparrow}\rangle$. Eventually, we have the effective pairing interaction $\bar{P}_\alpha = P_\alpha - \bar{P}_\alpha$ as well as the effective zero-frequency pair-pair correlation function $\bar{\mathcal{D}}_\alpha(\mathbf{i},\mathbf{j}) = \mathcal{D}_\alpha(\mathbf{i},\mathbf{j}) - \bar{\mathcal{D}}_\alpha(\mathbf{i},\mathbf{j})$. The appearance of negative effective pairing interaction may indicate that the pairing symmetry is suppressed by other competing states.

We also define the effective *zero-frequency* pair-pair structure factor for DQMC,

$$\bar{\mathcal{D}}_\alpha(\mathbf{q}) = \frac{1}{N_s}\sum_{\mathbf{i},\mathbf{j}} e^{i\mathbf{q}\cdot(\mathbf{i}-\mathbf{j})}\bar{\mathcal{D}}_\alpha(\mathbf{i},\mathbf{j}). \tag{6}$$

In particular, we use $P_d^{\mathrm{PDW}}(\mathbf{q}) \equiv \bar{\mathcal{D}}_d(\mathbf{q})$ to understand the effects of the charge-density modulation on the $d$-wave pair-density-wave (PDW) order. In the simulations, when the peak of $P_d^{\mathrm{PDW}}(\mathbf{q})$ is located at zero momentum, it indicates a lack of PDW state in the system. Otherwise, there may be a PDW state[50,51].

As magnetic excitation possibly plays an important role for the superconductivity mechanism in strong electron correlation systems, we also study the spin susceptibility in the $z$ direction at zero frequency in the $\mathcal{P}=3$ model,

$$\chi_s(\mathbf{q}) = \frac{1}{N_s}\int_0^\beta d\tau \sum_{\mathbf{i},\mathbf{j}} e^{i\mathbf{q}\cdot(\mathbf{i}-\mathbf{j})}\langle \mathrm{m}_{\mathbf{i}}(\tau)\mathrm{m}_{\mathbf{j}}(0)\rangle_T, \tag{7}$$

where $m_{\mathbf{i}}(\tau) = e^{H\tau}m_{\mathbf{i}}(0)e^{-H\tau}$ with $m_{\mathbf{i}}(0) = c^\dagger_{\mathbf{i}\uparrow}c_{\mathbf{i}\uparrow} - c^\dagger_{\mathbf{i}\downarrow}c_{\mathbf{i}\downarrow}$.

### DMRG method

At zero temperature, we employ the DMRG method to investigate the model Hamiltonian on a cylinder with 8, 192 SU(2) bases at most, equivalent to about 25, 000 U(1) bases, and guarantee that the truncation error is less than $10^{-5}$. We also examine the pairing-symmetry transition directly by investigating the static pair-pair structure factor

$$\mathcal{S}_\alpha(\mathbf{q}) = \frac{1}{N_s}\sum_{\mathbf{i},\mathbf{j}} e^{i\mathbf{q}\cdot(\mathbf{i}-\mathbf{j})}\left\langle \Delta^\dagger_\alpha(\mathbf{i},0)\Delta_\alpha(\mathbf{j},0)\right\rangle, \tag{8}$$

where the statistic average at a finite temperature and zero frequency in Eq. (6) is replaced with the ground-state expectation value at zero temperature here. Similarly, we also calculate the uncorrelated single-particle contribution $\tilde{\mathcal{S}}_\alpha(\mathbf{q})$ and define the effective static pair-pair structure factor as $\bar{\mathcal{S}}_\alpha(\mathbf{q}) = \mathcal{S}_\alpha(\mathbf{q}) - \tilde{\mathcal{S}}_\alpha(\mathbf{q})$. In the calculation, we target the lowest-energy zero-magnetic-momentum state with a specified even number of electrons. Thus, the number of electrons for any species is also preserved and the spin fluctuations remain negligible. In this work, we use the effective zero-momentum pair-pair structure factors $\bar{S}_s \equiv \bar{\mathcal{S}}_s(\mathbf{q}=(0,0))$ and $\bar{S}_d \equiv \bar{\mathcal{S}}_d(\mathbf{q}=(0,0))$, and the emerging peak of $\bar{\mathcal{S}}_d(\mathbf{q})$ at a finite momentum $\mathbf{q}\neq(0,0)$ to identify the $s$ and $d$-wave pairing as well as the $d$-wave PDW, respectively.

To clearly illustrate how the pairing-symmetry transition happens at zero temperature, we further decompose Cooper pair modes from the two-particle density matrix, defined as[52]

$$\rho(\mathbf{i}\boldsymbol{\delta}_l,\mathbf{j}\boldsymbol{\delta}_{l'}) = \left\langle \mathcal{C}^\dagger_{\mathbf{i}\boldsymbol{\delta}_l}\mathcal{C}_{\mathbf{j}\boldsymbol{\delta}_{l'}}\right\rangle, \tag{9}$$

where $\mathcal{C}_{\mathbf{i}\boldsymbol{\delta}_l}$ is consistent with the definition in Eq. (4). We exclude the overlapping parts for either $\mathbf{i}=\mathbf{j}$, or $\mathbf{i}=\mathbf{j}+\boldsymbol{\delta}_{l'}$, or $\mathbf{j}=\mathbf{i}+\boldsymbol{\delta}_l$, giving rise to the local contributions from density and spin correlations. Since $\rho$ is Hermitian, it can be diagonalized with real eigenvalues $\lambda_n$, that is,

$$\rho(\mathbf{i}\boldsymbol{\delta}_l,\mathbf{j}\boldsymbol{\delta}_{l'}) = \sum_n \lambda_n\zeta^*_n(\mathbf{i}\boldsymbol{\delta}_l)\zeta_n(\mathbf{j}\boldsymbol{\delta}_{l'}). \tag{10}$$

The eigenvector $\zeta_n(\mathbf{i}\boldsymbol{\delta}_l)$ are referred to as macroscopic wave functions of Cooper pair modes. The dominant mode with the largest eigenvalue is labeled by $n=0$.

### CPQMC method

To further demonstrate that the system may exhibit long-range superconducting correlations for the $s$ wave pairing, we also check the long-range part of the ground-state pair-correlation function using the CPQMC method[49,53]. The CPQMC method has been successfully used to calculate the ground-state energy and other observables in various systems[49,53]. We investigate the long-range superconducting correlations of dominant $s$-wave pairing symmetry by defining the pair-pair correlation function at zero temperature, which is written as

$$C_\alpha(\mathbf{r}) = \frac{1}{NN_r}\sum_{\mathbf{i},\mathbf{j}}\sum_{|\mathbf{j}-\mathbf{i}|=r}\left\langle \Delta^\dagger_\alpha(\mathbf{i},0)\Delta_\alpha(\mathbf{j},0)\right\rangle, \tag{11}$$

Here, $r$ is the distance between site $\mathbf{i}$ and site $\mathbf{j}$. The $N_r$ is the total number of distance $r$. Similarly, we also define the uncorrelated single-particle contribution $\tilde{C}_\alpha(\mathbf{r})$ and discuss the vertex contributions $\bar{C}_\alpha(\mathbf{r}) = C_\alpha(\mathbf{r}) - \tilde{C}_\alpha(\mathbf{r})$.

## Data availability

Data are available from the authors upon request.

## Code availability

DQMC and DMRG codes used for the data processing and other findings of this study are available upon request.

## References


1. Tranquada, J. M., Sternlieb, B. J., Axe, J. D., Nakamura, Y. & Uchida, S. Evidence for stripe correlations of spins and holes in copper oxide superconductors. *Nature* **375**, 561–563 (1995).
2. Abbamonte, P. et al. Spatially modulated "mottness" in $La_{2-x}Ba_xCuO_4$. *Nat. Phys.* **1**, 155–158 (2005).
3. Ghiringhelli, G. et al. Long-range incommensurate charge fluctuations in (Y, Nd)$Ba_2Cu_3O_{6+x}$. *Science* **337**, 821–825 (2012).
4. da Silva Neto, E. H. et al. Ubiquitous interplay between charge ordering and high-temperature superconductivity in cuprates. *Science* **343**, 393–396 (2014).
5. Fradkin, E. & Kivelson, S. A. Ineluctable complexity. *Nat. Phys.* **8**, 864–866 (2012).
6. Wang, Q. et al. Strong interplay between stripe spin fluctuations, nematicity and superconductivity in FeSe. *Nat. Mater.* **15**, 159–163 (2016).
7. Gu, Q. et al. Single particle tunneling spectrum of superconducting $Nd_{1-x}Sr_xNiO_2$ thin films. *Nat. Commun.* **11**, 6027 (2020).
8. Wang, B. Y. et al. Isotropic Pauli-limited superconductivity in the infinite-layer nickelate $Nd_{0.775}Sr_{0.225}NiO_2$. *Nat. Phys.* **17**, 473–477 (2021).
9. Harvey, S. P. et al. Evidence for nodal superconductivity in infinite-layer nickelates. Preprint at http://arxiv.org/abs/2201.12971 (2022).
10. Chow, L. E. et al. Pairing symmetry in infinite-layer nickelate superconductor. Preprint at http://arxiv.org/abs/2201.10038 (2022).
11. Ji, H. et al. Rotational symmetry breaking in superconducting nickelate $Nd_{0.8}Sr_{0.2}NiO_2$ films. *Nat. Commun.* **14**, 7155 (2023).
12. Cheng, B. et al. Evidence for d-wave superconductivity of infinite-layer nickelates from low-energy electrodynamics. *Nature Materials* (2024).
13. Yoshizawa, H. et al. Stripe order at low temperatures in $La_{2-x}Sr_xNiO_4$ with $0.289 \lesssim x \lesssim 0.5$. *Phys. Rev. B* **61**, R854–R857 (2000).
14. Zheng, L. et al. Emergent charge order in pressurized kagome superconductor $CsV_3Sb_5$. *Nature* **611**, 682–687 (2022).
15. Liu, Y. et al. Superconductivity under pressure in a chromium-based kagome metal. *Nature* **632**, 1032–1037 (2024).
16. Ding, X. et al. Critical role of hydrogen for superconductivity in nickelates. *Nature* **615**, 50–55 (2023).
17. Pelliciari, J. et al. Comment on newly found charge density waves in infinite layer nickelates. Preprint at http://arxiv.org/abs/2306.15086 (2023).
18. Tam, C. C. et al. Reply to "comment on newly found charge density waves in infinite layer nickelates". Preprint at http://arxiv.org/abs/2307.13569 (2023).
19. Parzyck, C. T. et al. Absence of $3a_0$ charge density wave order in the infinite-layer nickelate $NdNiO_2$. *Nat. Mater.* **23**, 486–491 (2024).
20. Keimer, B., Kivelson, S. A., Norman, M. R., Uchida, S. & Zaanen, J. From quantum matter to high-temperature superconductivity in copper oxides. *Nature* **518**, 179–186 (2015).

21. Arovas, D. P., Berg, E., Kivelson, S. A. & Raghu, S. The Hubbard model. *Annu. Rev. Condens. Matter Phys.* **13**, 239–274 (2022).
22. Dagotto, E. Correlated electrons in high-temperature superconductors. *Rev. Mod. Phys.* **66**, 763–840 (1994).
23. Scalapino, D. J. A common thread: The pairing interaction for unconventional superconductors. *Rev. Mod. Phys.* **84**, 1383–1417 (2012).
24. Fradkin, E., Kivelson, S. A. & Tranquada, J. M. Colloquium: theory of intertwined orders in high temperature superconductors. *Rev. Mod. Phys.* **87**, 457–482 (2015).
25. Zheng, B.-X. et al. Stripe order in the underdoped region of the two-dimensional Hubbard model. *Science* **358**, 1155–1160 (2017).
26. Huang, E. W. et al. Numerical evidence of fluctuating stripes in the normal state of high-Tc cuprate superconductors. *Science* **358**, 1161–1164 (2017).
27. Lin, H. Q. & Hirsch, J. E. Two-dimensional Hubbard model with nearest- and next-nearest-neighbor hopping. *Phys. Rev. B* **35**, 3359–3368 (1987).
28. Lichtenstein, A. I. & Katsnelson, M. I. Antiferromagnetism and *d*-wave superconductivity in cuprates: a cluster dynamical mean-field theory. *Phys. Rev. B* **62**, R9283–R9286 (2000).
29. Huang, E. W., Mendl, C. B., Jiang, H.-C., Moritz, B. & Devereaux, T. P. Stripe order from the perspective of the Hubbard model. *npj Quantum Mater.* **3**, 22 (2018).
30. Sénéchal, D., Lavertu, P.-L., Marois, M.-A. & Tremblay, A.-M. S. Competition between antiferromagnetism and superconductivity in high-$T_c$ cuprates. *Phys. Rev. Lett.* **94**, 156404 (2005).
31. Maier, T. A., Alvarez, G., Summers, M. & Schulthess, T. C. Dynamic cluster quantum Monte Carlo simulations of a two-dimensional Hubbard model with stripelike charge-density-wave modulations: interplay between inhomogeneities and the superconducting state. *Phys. Rev. Lett.* **104**, 247001 (2010).
32. Xu, H. et al. Coexistence of superconductivity with partially filled stripes in the Hubbard model. *Science* **384**, eadh7691 (2024).
33. Mondaini, R., Ying, T., Paiva, T. & Scalettar, R. T. Determinant quantum Monte Carlo study of the enhancement of *d*-wave pairing by charge inhomogeneity. *Phys. Rev. B* **86**, 184506 (2012).
34. Jiang, H.-C. & Kivelson, S. A. Stripe order enhanced superconductivity in the Hubbard model. *Proc. Natl Acad. Sci.* **119**, e2109406119 (2022).
35. Martin, I., Podolsky, D. & Kivelson, S. A. Enhancement of superconductivity by local inhomogeneities. *Phys. Rev. B* **72**, 060502 (2005).
36. Ding, X. et al. Cuprate-like electronic structures in infinite-layer nickelates with substantial hole dopings. *Natl Sci. Rev.* **11**, nwae194 (2024).
37. Sun, W. et al. Electronic structure of superconducting infinite-layer lanthanum nickelates. Preprint at http://arxiv.org/abs/2403.07344 (2024).
38. Zeng, S. et al. Phase diagram and superconducting dome of infinite-layer $Nd_{1-x}Sr_xNiO_2$ thin films. *Phys. Rev. Lett.* **125**, 147003 (2020).
39. Li, D. et al. Superconducting dome in $Nd_{1-x}Sr_xNiO_2$ infinite layer films. *Phys. Rev. Lett.* **125**, 027001 (2020).
40. Wu, T. et al. Magnetic-field-induced charge-stripe order in the high-temperature superconductor $YBa_2Cu_3O_y$. *Nature* **477**, 191–194 (2011).
41. Badoux, S. et al. Critical doping for the onset of fermi-surface reconstruction by charge-density-wave order in the cuprate superconductor $La_{2-x}Sr_xCuO_4$. *Phys. Rev. X* **6**, 021004 (2016).
42. Blankenbecler, R., Scalapino, D. J. & Sugar, R. L. Monte Carlo calculations of coupled boson-fermion systems. i. *Phys. Rev. D.* **24**, 2278–2286 (1981).
43. White, S. R. et al. Numerical study of the two-dimensional Hubbard model. *Phys. Rev. B* **40**, 506–516 (1989).
44. Ma, T., Zhang, L., Chang, C.-C., Hung, H.-H. & Scalettar, R. T. Localization of interacting Dirac fermions. *Phys. Rev. Lett.* **120**, 116601 (2018).
45. Zhang, L., Ma, T., Costa, N. C., dos Santos, R. R. & Scalettar, R. T. Determinant quantum Monte Carlo study of exhaustion in the periodic anderson model. *Phys. Rev. B* **99**, 195147 (2019).
46. Mondaini, R., Tarat, S. & Scalettar, R. T. Quantum critical points and the sign problem. *Science* **375**, 418–424 (2022).
47. White, S. R., Scalapino, D. J., Sugar, R. L., Bickers, N. E. & Scalettar, R. T. Attractive and repulsive pairing interaction vertices for the two-dimensional Hubbard model. *Phys. Rev. B* **39**, 839–842 (1989).
48. Ma, T., Lin, H.-Q. & Hu, J. Quantum Monte Carlo study of a dominant *s*-wave pairing symmetry in iron-based superconductors. *Phys. Rev. Lett.* **110**, 107002 (2013).
49. Huang, T., Zhang, L. & Ma, T. Antiferromagnetically ordered mott insulator and *d*+*id* superconductivity in twisted bilayer graphene: a quantum Monte Carlo study. *Sci. Bull.* **64**, 310–314 (2019).
50. Agterberg, D. F. et al. The physics of pair-density waves: cuprate superconductors and beyond. *Annu. Rev. Condens. Matter Phys.* **11**, 231–270 (2020).
51. Huang, K. S., Han, Z., Kivelson, S. A. & Yao, H. Pair-density-wave in the strong coupling limit of the Holstein-Hubbard model. *npj Quantum Mater.* **7**, 17 (2022).
52. Wietek, A. Fragmented cooper pair condensation in striped superconductors. *Phys. Rev. Lett.* **129**, 177001 (2022).
53. Zhang, S., Carlson, J. & Gubernatis, J. E. Constrained path quantum Monte Carlo method for fermion ground states. *Phys. Rev. Lett.* **74**, 3652–3655 (1995).


## Acknowledgements

We thank Rubem Mondaini and Xuefeng Zhang for useful discussions. This work was supported by National Natural Science Foundation of China (Grants No. 12088101 and No. 12474218), National Key Research and Development of China (Grant No. 2022YFA1402400), the NSAF (Grant No. U2230402) and Beijing Natural Science Foundation (Grant No. 1242022). The numerical simulations in this work were performed at the HSCC of Beijing Normal University and Tianhe2-JK in Beijing Computational Science Research Center.

## Author contributions

B.H. convinced the project. B.H., H.Q.L., S.H., and T.M. directed the project. C.C., R.M., Y.L., T.M., and H.Q.L. developed the DQMC and CPQMC codes and performed the simulations. P.Z. and S.H. developed the DMRG code and performed the simulations. X.S. contributed to the DFT calculations. C.C., S.H., and B.H. prepared the manuscript. All authors discussed the results and contributed to the manuscript.

## Competing interests

The authors declare no competing interests.

## Additional information

**Supplementary information** The online version contains supplementary material available at https://doi.org/10.1038/s41467-024-53841-x.

**Correspondence** and requests for materials should be addressed to Shijie Hu, Tianxing Ma or Bing Huang.

**Peer review information** *Nature Communications* thanks the anonymous reviewers for their contribution to the peer review of this work. A peer review file is available.